JOURNAL OF APPLIED PHYSICS VOLUME 90, NUMBER 8 15 OCTOBER 2001

Quantitative C lattice site distributions in epitaxial $Ge_{1-y}C_y$/Ge(001) layers

J. D'Arcy-Gall,[a] D. Gall, I. Petrov, P. Desjardins,[b] and J. E. Greene
Materials Science Department and the Frederick Seitz Materials Research Laboratory, University of Illinois, 104 South Goodwin Avenue, Urbana, Illinois 61801

(Received 21 February 2001; accepted for publication 13 July 2001)

Epitaxial metastable $Ge_{1-y}C_y$ alloy layers with $y \leqslant 0.035$ were grown on Ge(001) from hyperthermal Ge and C atomic beams at deposition temperatures T_s of 250 and 300 °C. The use of hyperthermal beams allows us to controllably vary the concentration of C incorporated as Ge–C split interstitials. $Ge_{1-y}C_y$ layers grown with incident Ge-atom energy distributions corresponding to $\leqslant 0.14$ lattice displacement per incident atom (dpa) are in a state of in-plane tension and contain significant concentrations of C atoms incorporated in substitutional sites. Increasing the dpa to 0.24 yields layers in compression with C incorporated primarily as Ge–C split interstitials. *Ab initio* density functional calculations of the formation energies and strain coefficients associated with C atomic arrangements in Ge show that configurations containing multiple C atoms, referred to collectively as C nanoclusters, are energetically more favorable than substitutional C and Ge–C split interstitials and yield a nearly zero average strain. In contrast, substitutional C and Ge–C split interstitials produce large tensile and compressive strains, respectively. Using the calculated strain coefficients, measured layer strains obtained from high-resolution reciprocal lattice maps, and substitutional C concentrations determined by Raman spectroscopy, we obtain the fraction of C atoms incorporated in substitutional, Ge–C split interstitial, and nanocluster sites as a function of the total C concentration y and T_s. We find that at low y and T_s values, all C atoms are incorporated in single-C configurations: substitutional C and Ge–C split interstitials. Their relative concentrations are controlled by the dpa through the production of near-surface Ge self-interstitials which are trapped by substitutional C atoms to form Ge–C split interstitials. Increasing y and T_s, irrespective of the dpa, leads to an increase in the fraction of C nanoclusters, while the fractions of substitutional C and Ge–C split interstitials decrease, due to the higher C–C encounter probability at the growth surface. © *2001 American Institute of Physics.* [DOI: 10.1063/1.1402137]

I. INTRODUCTION

C-containing group-IV alloys are of technological and scientific interest due to the potential they offer for both band-gap and strain-state engineering of layers used in microelectronic and optoelectronic devices compatible with Si integrated circuit technology. There are, however, severe challenges associated with their growth. First, the equilibrium solubility of C in Si and Ge is extremely low, $\simeq 10^{17}$ and 10^8 cm^{-3}, respectively.[1] Low-temperature growth under highly kinetically constrained conditions is required to take advantage of the fact that surface solubilities are orders of magnitude larger than bulk values,[2] while simultaneously inhibiting phase separation during deposition. Another obstacle to be overcome is the large lattice constant mismatch, 34% and 37%, between diamond ($a_C = 3.5668$ Å) and the common group-IV semiconductors Si ($a_{Si} = 5.4310$ Å) and Ge ($a_{Ge} = 5.6576$ Å). Moreover, C atoms tend to incorporate in nonsubstitutional lattice sites and/or to form defect complexes in Si and Ge.

There are few reports of the successful growth of metastable $Ge_{1-y}C_y$ alloys on Ge(001). Duschl *et al.*[3] employed solid-source molecular beam epitaxy (MBE) to grow 30 periods of 30-Å-$Ge_{1-y}C_y$/100-Å-Ge superlattices with $y = 0.012$ and 0.021 at temperatures T_s of 200 and 300 °C. The authors reported that only 30% and 10% of the total C content occupied substitutional sites at 200 and 300 °C, respectively, based upon strain values obtained from x-ray diffraction measurements and the assumption that nonsubstitutional C atoms do not induce strain on the Ge lattice. Dashiell *et al.*[4] demonstrated in-plane tension in $Ge_{1-y}C_y$ layers grown by MBE at $T_s = 275$ °C, but did not provide the total incorporated C concentrations.

Yang *et al.*[5] reported the growth of epitaxial $Ge_{0.95}C_{0.05}$ on Ge(001) by MBE at $T_s = 200$ °C and noted that the layers were highly defective with rough 113 facetted surfaces. Raman spectroscopy indicated that only a small fraction of the C was in substitutional sites giving rise to a local vibrational mode at 530 cm^{-1} (Ref. 6). The latter is in good agreement with an investigation by Hoffman and coworkers[7] who used ion channeling and infrared absorption spectroscopy analyses to characterize Ge wafers implanted with $^{12}C^+$ and $^{13}C^+$ ions at energies and doses chosen to provide a uniformly doped 0.7-μm-thick region with $y = 0.007$. They observed a Ge–C stretch mode at a frequency of 531 cm^{-1}, consistent with values between 516 and 563 cm^{-1} obtained from their local density functional calculations of the vibrational mode frequencies of substitutional C in Ge. Analyses of channeling

[a]Electronic mail: darcy@uiuc.edu
[b]Present address: Département de génie physique et de génie des matériaux, École Polytechnique de Montréal, C.P. 6079, Succ. Centre-Ville, Montréal, Québec, Canada H3C 3A7.

 © 2001 American Institute of Physics

Downloaded 28 Sep 2001 to 130.126.25.129. Redistribution subject to AIP license or copyright, see http://ojps.aip.org/japo/japcr.jsp

rocking curves around the ⟨100⟩, ⟨110⟩, and ⟨111⟩ axes suggested that up to $31\pm3\%$ of the incorporated C was in substitutional sites.

$Ge_{1-y}C_y$ alloys have received even less theoretical attention. Most reports[8,9] consider only C incorporation in substitutional sites and ignore nonsubstitutional C configurations. Although the most stable configuration for C atoms in the Si lattice is the substitutional site,[10] we have shown, using *ab initio* density-functional calculations, that the situation is rather different in the case of Ge.[11] For fully coherent epitaxial $Ge_{1-y}C_y$ layers on Ge(001), substitutional C atoms are energetically less favorable than configurations containing multiple C atoms, referred to collectively as nanoclusters. Our calculations also indicate that the [001]-oriented Ge–C split interstitial is the most stable interstitial C configuration in Ge and that while substitutional C atoms exert a large tensile strain in the Ge lattice, C atoms incorporated in Ge–C split interstitial sites yield a large compressive strain.

We recently reported the growth, at $T_s=300\,°C$, of $Ge_{0.990}C_{0.010}$/Ge(001) alloys from hyperthermal beams with typical average energies of 13–16 eV.[12] We showed that the layer strain is controllably varied through changes in the incident Ge-atom energy distribution and that the ratio of incorporated C residing in Ge–C split interstitials to that in substitutional sites is directly correlated with the number of lattice displacements in the growing film per incident hyperthermal atom (dpa) calculated using TRIM[13] Monte Carlo simulations (Ref. 12). Layers grown with dpa values $\leqslant 0.14$ are in tension with large substitutional concentrations while layers grown with dpa>0.17 exhibit increasingly higher compressive strain due to an increasing concentration of Ge–C split interstitials. Here we use this finding, as described below, to obtain new insights into C incorporation reaction paths.

In this article we present the results of a series of experiments, combined with density functional calculations, designed to probe C incorporation pathways into the Ge lattice during the growth of epitaxial $Ge_{1-y}C_y$/Ge(001) alloys. We vary not only the total C concentration y and film growth temperature T_s, but the Ge–C split interstitial concentration as well by utilizing the results of Ref. 12 and varying the dpa during deposition through changes in the incident Ge-atom energy distribution. We employ a combination of Raman spectroscopy, high-resolution reciprocal lattice mapping (HRRLM), cross-sectional transmission electron microscopy (XTEM), and *ab initio* calculations of the strains and formation energies associated with possible C configurations in Ge to determine changes in C lattice site distributions as a function of y, T_s, and dpa and from this deduce C incorporation pathways during film growth.

We find that at low y and T_s values, all C atoms are incorporated in single-C configurations: substitutional C and Ge–C split interstitials. The relative concentrations of these two species are controlled by the dpa through the near-surface production of Ge self-interstitials which become trapped by substitutional C atoms to form Ge–C split interstitials. Layers grown with a "low" dpa of 0.14 contain significant fractions of substitutional C atoms (up to 67%), while alloys grown with a "high" dpa (0.24) have negligible substitutional C fractions. As y and T_s increase, irrespective of the dpa, the C–C encounter probability on the growth surface increases giving rise to C incorporation in nanocluster sites with correspondingly lower C fractions occupying single-C configurations. C incorporation in nanoclusters is favorable since their formation energy is well below that of either substitutional C or Ge–C split interstitials.

II. EXPERIMENTAL PROCEDURE

All films were grown in a multichamber ultrahigh-vacuum (UHV) load-locked stainless-steel system. The growth chamber is cryopumped with a base pressure of 1×10^{-10} Torr and contains facilities for *in situ* reflection high-energy electron-diffraction.[14] Hyperthermal Ge and C neutral atom beams were obtained by simultaneously sputtering an undoped float-zone Ge wafer and a high-purity C target with either 450 or 900 eV Kr^+ ions, generated by two separate UHV modified Kaufman-type double-grid multiaperture broad-beam sources with provisions for *in situ* spatial adjustment. The chamber pressure during deposition is 1.2×10^{-4} Torr.

The sputtering system geometry described in Ref. 15, together with the use of the higher-mass Kr instead of Ar, minimizes the flux of energetic backscattered particles. Each ion beam is focused by a postextraction unipotential electrostatic lens that also acts as a mirror to prevent electron backstreaming from the neutralization device. Space-charge spreading is suppressed in each source immediately upon emerging from the final lens aperture by electron injection from a circular thermionic W filament. The filament is positioned external to the beam in order to eliminate W contamination. A detailed discussion of the design, construction, and operation of the ion sources is presented elsewhere.[15]

Incident hyperthermal Ge and C beam fluxes, and hence $Ge_{1-y}C_y$ film compositions, are controlled through the choice of beam currents from each ion gun. The Ge and C beams are both incident at 20° to the substrate surface normal with average energies per atom of 13 and 17 eV, respectively, as determined from TRIM Monte Carlo simulations[12] for 450 eV Kr^+ ion sputtering. These values increase to 16 and 24 eV for 900 eV Kr^+ ions. Even though the increase in the average energy per atom is relatively small, we showed in Ref. 12 that the corresponding dpa increases by almost a factor of 2 due to an increase in the high-energy tail of the Ge-atom energy distribution.

The substrates are polished $1.5\times1.5\,cm^2$ Sb-doped Ge(001) wafers with room-temperature resistivities of 1–20 $\Omega\,cm$ ($n=1\times10^{15}-6\times10^{13}\,cm^{-3}$). Substrate cleaning consists of ultrasonic degreasing, rinsing in deionized water to remove the native oxide, and oxidation by a UV-ozone process.[16] The wafers are then bonded to the substrate platen with In and immediately inserted into the UHV system. Final substrate preparation comprises degassing at 200 °C for 10 min and desorption of the oxide layer at 450 °C for 15 min. 1000-Å-thick Ge(001) buffer layers are deposited at $T_s=300\,°C$ followed by the growth of ≃2000-Å-thick $Ge_{1-y}C_y$ alloy layers at T_s values of either 250 or 300 °C.

Downloaded 28 Sep 2001 to 130.126.25.129. Redistribution subject to AIP license or copyright, see http://ojps.aip.org/japo/japcr.jsp

The deposition rates are 0.5 and 1.4 Å s^{-1} with $E_{Kr}=450$ and 900 eV, respectively.

$Ge_{1-y}C_y$ film compositions were determined using a Cameca IMS-5F secondary ion mass spectrometer (SIMS) operated with a 10 kV Cs^+ primary ion beam. Quantification was obtained by comparison to C-implanted Ge(001) reference wafers. SIMS results showed that C concentrations in the alloys increased linearly with the Kr^+ ion current at the C target and are constant as a function of depth in all layers, irrespective of y or T_s.

A Philips CM12 microscope operated at 120 kV was used for XTEM examinations. Specimens were prepared by mechanical thinning followed by ion milling as described in Ref. 17. Lattice constants $a_\perp$ along the growth direction, in-plane lattice constants $a_\parallel$, and residual strains were determined from HRRLMs around asymmetric reflections. The measurements were performed in a Philips X-Pert MRD diffractometer using Cu $K\alpha_1$ radiation ($\lambda=1.540\,597$ Å) from a four-crystal Ge(220) monochromator. A two-crystal Ge(220) analyzer was placed in front of the detector and a series of ω–2θ scans was acquired at different ω offsets (ω is the x-ray angle of incidence and θ is the Bragg diffraction angle).

Raman measurements were performed at room temperature using the 5145 Å line from an Ar^+ ion laser. The 40 mW laser beam was incident at 60° to the sample normal and focused to a spot size of $\simeq 300$ μm. The penetration depth at this wavelength is $\simeq 160$ Å,[18] much smaller than the alloy layer thickness. A three-stage 0.8 m SPEX spectrometer equipped with a two-dimensional charged-coupled device array was used to collect the signal perpendicular to the sample surface. Wavelength calibration was done using a Ne lamp.

III. C CONFIGURATIONS IN $Ge_{1-y}C_y$/Ge(001)

Ab initio density functional methods were used to calculate the formation energies U and strain coefficients α of C lattice configurations in $Ge_{1-y}C_y$ alloys. The calculations were performed using the Vienna *ab initio* simulation package (VASP)[19] which employs ultrasoft Vanderbilt-type pseudopotentials[20] and a plane-wave basis set to determine the Kohn–Sham ground state using the generalized gradient approximation (GGA) of Perdew and Wang.[21]

$Ge_{1-y}C_y$ configurations were calculated in the neutral charge state using 64-atom tetragonal supercells for which $a_x=a_y=a_\parallel=a_{Ge}$, where a_{Ge} is the relaxed bulk Ge lattice constant. This corresponds to the pseudomorphic growth of $Ge_{1-y}C_y$ on Ge(001) where, for a given C lattice configuration, the lattice constant perpendicular to the film surface $a_\perp$ varies linearly with alloy concentration. Equilibrium total energies and strain coefficients were obtained for each $Ge_{1-y}C_y$ configuration by relaxing the ionic positions using a conjugate-gradient algorithm for a minimum set of three different unit cell sizes. Details concerning the computational procedure are described in Ref. 11.

Figure 1(a) shows the most stable configuration involving a single C atom. Substitutional C has a formation energy $U_{sub}=2.40$ eV and a strain coefficient α_{sub} of -0.71 (the negative sign corresponds to tension). The strain coefficient

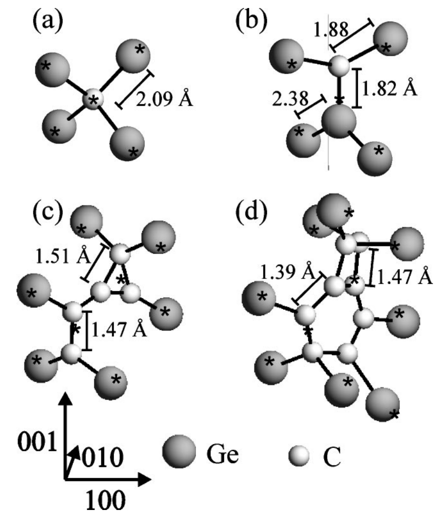

FIG. 1. Relaxed C configurations in pseudomorphic $Ge_{1-y}C_y$/Ge(001) with in-plane lattice constants $a_x=a_y=a_{Ge}$: (a) substitutional C, (b) Ge–C split interstitial, (c) five C atoms occupying two substitutional sites, and (d) eight C atoms occupying two substitutional sites. The asterisks represent the Ge equilibrium positions.

α for a given C lattice configuration is defined by the strain state of a commensurate $Ge_{1-y}C_y$ layer on Ge(001) through the expression

$$\alpha=\frac{1}{y}\left(\frac{a_\perp-a_{Ge}}{a_{Ge}}\right), \tag{1}$$

where y is the total C concentration. The [001]-oriented Ge–C split interstitial [Fig. 1(b)], formed by the capture of a Ge self-interstitial by a substitutional C, is the most stable interstitial C configuration in Ge with $U_{split}=4.18$ eV and $\alpha_{split}=0.95$ (compression). In Sec. IV C, we provide experimental evidence for C incorporation in both the substitutional and split interstitial configurations with the relative concentrations depending on film deposition conditions.

We showed in Ref. 11 that lattice configurations involving two and three C atoms can be significantly more stable than the substitutional C configuration [Fig. 1(a)]. Here we determine formation energies and strain coefficients for ≈ 50 different nanocluster configurations in which the number of C atoms N_C is between 2 and 8. Example nanoclusters are shown in Figs. 1(c) and 1(d). Figure 1(c) is the most stable configuration containing five C atoms and occupying two substitutional sites in the Ge lattice. The lowest energy configuration with eight C atoms on two sites [Fig. 1(d)] contains a distorted six-membered C ring.

The formation energy per C atom, $\tilde{U}=U/N_C$, of the most stable configuration for each type of site (i.e., C atoms occupying an interstitial site, or one, two, or three substitutional sites) is plotted in Fig. 2(a) as a function of N_C. The results exhibit a clear trend with $\tilde{U}$ continuously decreasing with increasing N_C. For example, the most stable configuration with $N_C=2$ is 0.51 eV less stable than the lowest energy configuration with $N_C=3$, which is in turn less stable than the lowest energy configuration with $N_C=4$, and so on.

We note that for configurations with $N_C \geqslant 5$, the total number of possible atomic arrangements is too large to cal-

Downloaded 28 Sep 2001 to 130.126.25.129. Redistribution subject to AIP license or copyright, see http://ojps.aip.org/japo/japcr.jsp

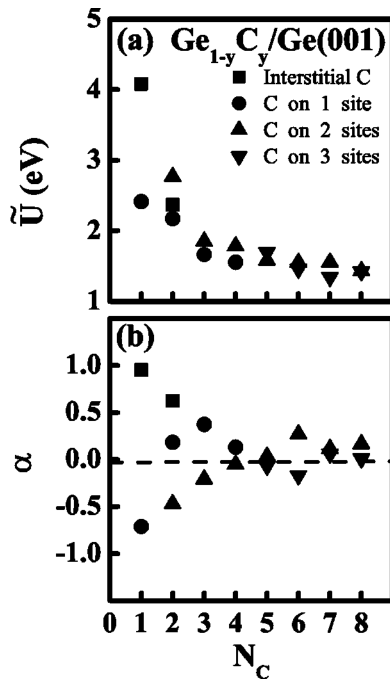

FIG. 2. (a) Formation energy per C atom $\tilde{U}$ and (b) strain coefficient α vs the number of C atoms N_C per configuration and the number of Ge lattice sites they occupy in pseudomorphic $Ge_{1-y}C_y$/Ge(001). For each value of N_C we plot $\tilde{U}$ and α corresponding to the most stable configurations occupying the split interstitial, and one, two, and three substitutional lattice sites.

culate. Thus, for each higher N_C value, we make reasonable choices based upon the results for lower N_C configurations. The data plotted in Fig. 2(a) for $N_C \geqslant 5$ may therefore not correspond to global energy minima. That is, the actual formation energies for $N_C \geqslant 5$ may even be lower. Nevertheless, the overall set of results is consistent and conclusively shows that $\tilde{U}$ continuously decreases with increasing N_C indicating that C in Ge has a strong tendency to form nanoclusters.

Figure 2(b) is a plot of calculated strain coefficients α as a function of N_C for the C configurations corresponding to the formation energies $\tilde{U}$ in Fig. 2(a). The absolute value of the strain coefficients is largest for single-C configurations ($N_C = 1$), with $\alpha_{split} = 0.95$ and $\alpha_{sub} = -0.71$, and decreases dramatically to approximately zero for configurations with $N_C \geqslant 2$. This trend is not surprising since α is defined in Eq. (1) as the strain per C concentration y.

Knowledge of α for each configuration is essential for carrying out quantitative analyses of the layer strain in terms of C lattice site distributions. As discussed in Secs. IV and V, we use a combination of Raman spectroscopy and HRRLM to provide experimental evidence for C incorporation in substitutional and Ge–C split interstitial sites in our $Ge_{1-y}C_y$ layers. Analyses of layer strains measured in the full set of samples suggest that C configurations with $N_C \geqslant 2$ (for convenience, collectively termed C nanoclusters) are also present in $Ge_{1-y}C_y$. In order to simplify quantitative analyses, we assign the nanoclusters an effective strain coefficient of $\alpha_{cluster} = 0$. Based upon the calculated strain for $N_C = 2$ we estimate this adds an uncertainty in the determination of C lattice site distributions of less than 12%.

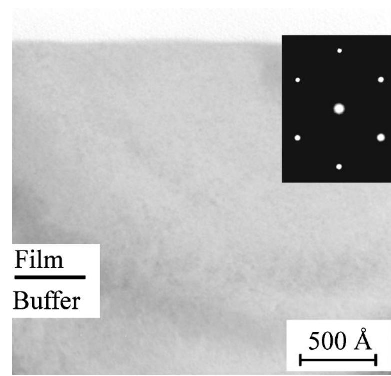

FIG. 3. A bright-field XTEM image obtained with diffraction vector $\bar{g} = 220$ near [110] from a fully coherent $Ge_{0.975}C_{0.025}$ alloy layer grown on Ge(001) at $T_s = 250\,°C$ with the dpa value of 0.24. A 110 selected-area electron diffraction pattern is shown in the inset.

The out-of-plane lattice constant $a_\perp$ for fully coherent $Ge_{1-y}C_y$ films on Ge(001) can be expressed as a linear combination of the strains associated with C in each lattice configuration,

$$a_\perp = a_{Ge}(1 + \alpha_{sub} y_{sub} + \alpha_{split} y_{split} + \alpha_{cluster} y_{cluster}) \tag{2}$$

where

$$y = y_{sub} + y_{split} + y_{cluster}. \tag{3}$$

y_{sub}, y_{split}, and $y_{cluster}$ are the C atom concentrations incorporated in substitutional, split-interstitial, and nanocluster sites, respectively.

IV. EXPERIMENTAL RESULTS

Epitaxial $Ge_{1-y}C_y$ layers were grown on Ge(001) from Ge and C hyperthermal beams corresponding to a ''low'' dpa value of 0.14 and a ''high'' dpa value of 0.24. For each set of growth conditions, C incorporation pathways were probed by varying the total C concentration between 0.07 and 3.5 at. % for film growth temperatures T_s of 250 and 300 °C. We show, using a combination of XTEM and HRRLM, that all layers are high-quality single crystals with no detectable extended defects or C precipitates. In order to determine the fractional C concentrations incorporated into substitutional, Ge–C split interstitial, and nanocluster sites as a function of the total C concentration y, film growth temperature, and dpa, we first measure y by SIMS and then obtain the substitutional C concentrations from Raman scattering results. The next step is to determine $a_\perp$ values from HRRLM and, finally, we substitute y, y_{sub}, $a_\perp$, and calculated α values into Eqs. (2) and (3) and solve for y_{split} and $y_{cluster}$.

A. Microstructure

Figure 3 is a typical bright-field XTEM image, obtained using the diffraction vector $\bar{g} = 220$ near the 110 zone axis, from a $Ge_{0.975}C_{0.025}$ layer grown at $T_s = 250\,°C$ with the high dpa of 0.24. The film contains no observable stacking faults, dislocations, or evidence for C precipitates (detection limit $\simeq 50$ Å). The surface is flat to within the resolution of the TEM and the film/buffer layer interface is abrupt (determined from $\bar{g} = 004$ images, not shown). The 110 zone axis

Downloaded 28 Sep 2001 to 130.126.25.129. Redistribution subject to AIP license or copyright, see http://ojps.aip.org/japo/japcr.jsp

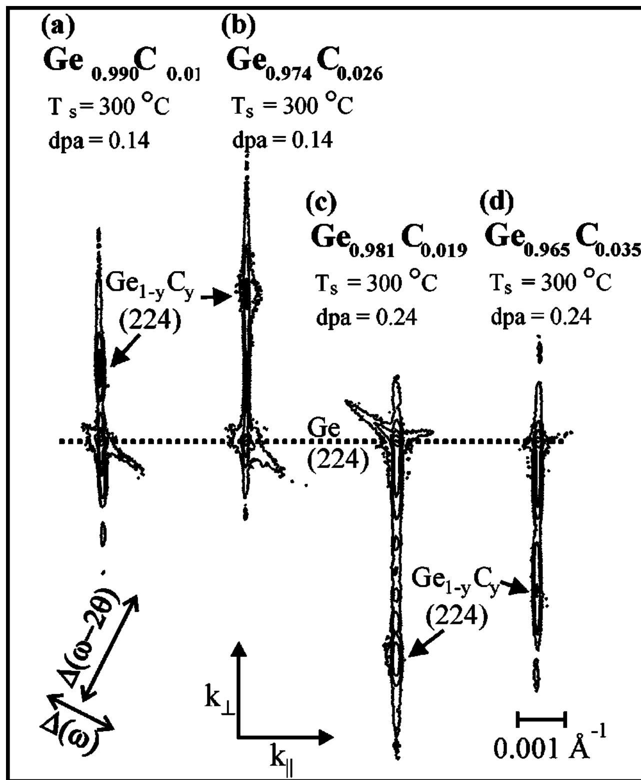

FIG. 4. HRRLMs around the asymmetric 224 Bragg peaks from $Ge_{1-y}C_y$/Ge(001) alloy layers deposited at $T_s = 300\,°C$: (a) $Ge_{0.990}C_{0.010}$, dpa=0.14; (b) $Ge_{0.974}C_{0.026}$, dpa=0.14; (c) $Ge_{0.981}C_{0.019}$, dpa=0.24; and (d) $Ge_{0.965}C_{0.035}$, dpa=0.24.

selected-area electron-diffraction pattern in the inset consists of single-crystal reflections with symmetric intensities.

All alloy layers are completely coherent with their substrates as determined from XTEM and HRRLM analyses. Representative reciprocal lattice maps around the asymmetric 224 reflection from $Ge_{1-y}C_y$ layers grown using low and high dpa values are presented in Fig. 4. Diffracted intensities are plotted as isointensity contours as a function of the reciprocal lattice vectors $k_{\parallel}$ parallel and $k_{\perp}$ perpendicular to the surface. The substrate and the film peaks are, for all samples, perfectly aligned along the $k_{\parallel}$ direction indicating negligible in-plane strain relaxation to within a detection limit of 1×10^{-5}. The layer peak appears below (above) the Ge substrate peak for alloy films in compression (tension). The diffraction contours in Fig. 4 are nearly symmetric with the exception of the elongation along the growth direction due to finite-thickness effects.

The HRRLMs in Figs. 4(a) and 4(b) were obtained from $Ge_{0.990}C_{0.010}$ and $Ge_{0.974}C_{0.026}$ alloys, respectively, grown at $T_s = 300\,°C$ with the low dpa value of 0.14. Both layers are under tensile strain with out-of-plane lattice constants $a_{\perp} = 5.649$ Å for $y = 0.010$ and $a_{\perp} = 5.636$ Å for $y = 0.026$, suggesting that a significant fraction of the incorporated C atoms reside in substitutional sites. Figures 4(c) and 4(d) are reciprocal lattice maps from $Ge_{1-y}C_y$ layers grown at $T_s = 300\,°C$ with the high dpa, 0.24. $Ge_{0.981}C_{0.019}$ [Fig. 4(c)] and $Ge_{0.965}C_{0.035}$ [Fig. 4(d)] alloy layers are both in compression with $a_{\perp} = 5.694$ and 5.682 Å, respectively. This indicates, based upon our calculated strain coefficients in Sec. III, that a large fraction of C atoms incorporated in the high dpa samples occupy split interstitial sites. Numerous interference fringes are clearly visible as periodic intensity contours positioned along $k_{\perp}$ in Fig. 4(c), with the periodicity corresponding to a layer thickness of 1750 Å in good agreement with the value expected from growth rate calibrations. The presence of the fringes in all HRRLMs is indicative of the high structural quality of the $Ge_{1-y}C_y$ layers, consistent with XTEM results.

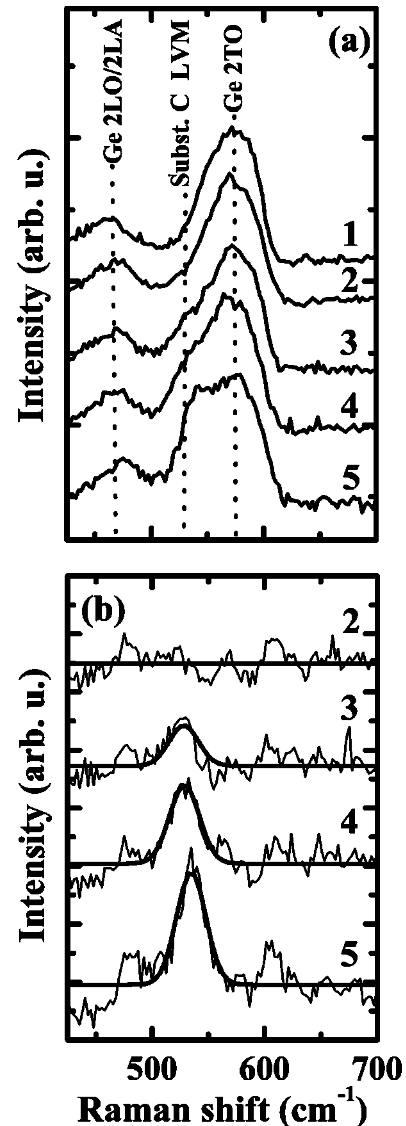

FIG. 5. (a) Raman spectra obtained from (1) a Ge(001) substrate and (2)–(5) $Ge_{1-y}C_y$/Ge(001) alloys deposited at $T_s = 300\,°C$. (b) Difference spectra from (2) $Ge_{0.990}C_{0.010}$, dpa=0.24; (3) $Ge_{0.997}C_{0.003}$, dpa=0.14; (4) $Ge_{0.990}C_{0.010}$, dpa=0.14; and (5) $Ge_{0.974}C_{0.026}$, dpa=0.14. The thick lines in (b) are Gaussian fits to the experimental data.

B. Substitutional C concentration

Substitutional C atoms in the Ge lattice give rise to a local vibrational mode (LVM) which has previously been reported to occur at approximately 530 cm^{-1} in $Ge_{1-y}C_y(001)$.[6,7] The curve labeled 1 in Fig. 5(a) is a reference Raman spectrum, over the Stokes shift range from 425 to 700 cm^{-1}, from a Ge substrate. In agreement with Ge

Downloaded 28 Sep 2001 to 130.126.25.129. Redistribution subject to AIP license or copyright, see http://ojps.aip.org/japo/japcr.jsp

phonon dispersion curves,[22] we relate the peak near 575 cm^{-1} to the Ge two-phonon transverse optical (2TO) mode, while the feature near 467 cm^{-1} corresponds to a convolution of the Ge two-phonon longitudinal optical and acoustic (2LO/2LA) modes.

Curves 2–5 in Fig. 5(a) are typical Raman spectra from $Ge_{1-y}C_y$ alloy layers grown at $T_s = 300\,°C$. Spectrum 2, which is obtained from a $Ge_{0.990}C_{0.010}$ layer grown with the high dpa value, is essentially identical to that of the Ge substrate and does not exhibit any C-related features. Spectra 3, 4, and 5 correspond to $Ge_{1-y}C_y$ layers grown with the low dpa and having y values which increase from 0.003 (curve 3) to 0.010 (curve 4) to 0.026 (curve 5). In addition to the two peaks already assigned to bulk Ge, spectra 3–5 exhibit an additional C-related feature, appearing as a broad shoulder, whose intensity increases with increasing y, on the low energy side of the Ge 2TO peak. To quantify this C-related feature, all spectra were normalized to the Ge 2TO peak intensity and the pure Ge spectra subtracted. The resulting $Ge_{1-y}C_y$ alloy difference spectra are plotted in Fig. 5(b).

Curve 2 in Fig. 5(b), corresponding to a $Ge_{0.990}C_{0.010}$ layer grown with the high dpa value, exhibits no evidence of C-related features, indicating that the substitutional C concentration in this layer is negligible. In contrast, the C-related peaks in spectra 3–5 were well fit using a Gaussian function centered at 531 cm^{-1}. We attribute this peak to the local vibrational mode for substitutional C in Ge, in agreement with previous reports.[6,7] The intensity of, and integrated area under, the C peak increase with y, showing that the substitutional C concentration in layers grown with the low dpa value increases with the total C concentration.

Obtaining a quantitative measure of the substitutional C concentration in our $Ge_{1-y}C_y$ alloys requires reference samples. For this, we use alloy layers grown with the low dpa value and having very low total C concentrations. Layer strain analyses in high dpa samples (see Fig. 7, next section) show that for alloys with $y \lesssim 0.005$ grown at $T_s = 300\,°C$, C is incorporated only in Ge–C split interstitial sites. Since the reaction path for nanocluster formation depends solely on the total C concentration and T_s, we expect that C will also incorporate only in single-C configurations in $Ge_{1-y}C_y$ alloys grown at the low dpa with very low C concentrations. However, in this case C will occupy substitutional, in addition to split interstitial, sites. These alloys can thus serve as our reference samples since we can obtain the substitutional concentration y_{sub} from the measured out-of-plane lattice constant combined with calculated strain coefficients.

Using Eqs. (2) and (3), we determine that the $Ge_{0.997}C_{0.003}$ layer grown at $T_s = 300\,°C$ with a dpa of 0.14 has a substitutional C concentration $y_{sub} = 0.002$. Thus the fraction $\xi_{sub} = y_{sub}/y$ of incorporated C atoms occupying substitutional sites in our reference samples is $67 \pm 7\%$, with the remaining C occupying split interstitial sites.

Figure 6 is a plot of the substitutional C concentration y_{sub} as a function of the total incorporated C concentration y in $Ge_{1-y}C_y$ alloys grown at 250 and 300 °C with both high and low dpa values. For all $Ge_{1-y}C_y$ layers, $y_{sub} < y$. For layers grown at $T_s = 300\,°C$ with the low dpa value of 0.14 (closed squares), the substitutional C concentration increases from $y_{sub} = 0.002$ with $y = 0.003$ to $y_{sub} = 0.007$ with $y = 0.035$. Nevertheless, the substitutional fraction ξ_{sub} decreases with increasing y (see Sec. V and Fig. 8) due to a rapid increase in the fraction of C incorporated in nanoclusters. Lowering the growth temperature to $T_s = 250\,°C$ with the low dpa (open squares) yields $Ge_{1-y}C_y$ alloys with slightly larger substitutional fractions.

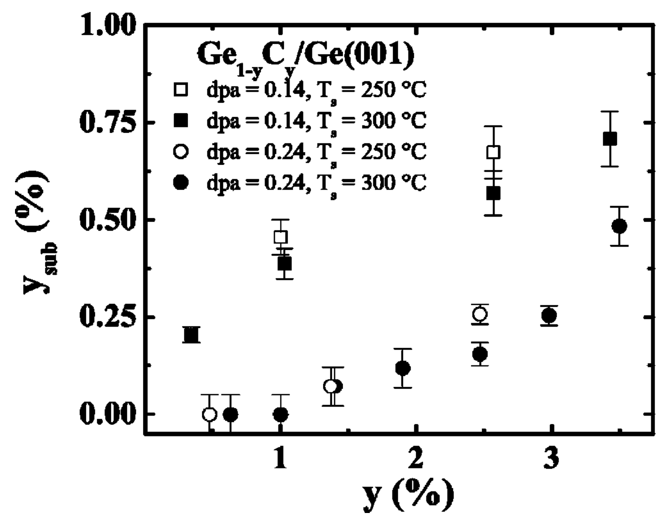

FIG. 6. Substitutional C concentration y_{sub}, as determined by Raman spectroscopy, in $Ge_{1-y}C_y$ alloys as a function of the total C concentration y. Open squares: dpa=0.14, $T_s = 250\,°C$; closed squares: dpa=0.14; $T_s = 300\,°C$; open circles: dpa=0.24, $T_s = 250\,°C$; and closed circles: dpa =0.24, $T_s = 300\,°C$.

Increasing the dpa to 0.24 decreases the substitutional C concentration y_{sub} in $Ge_{1-y}C_y$ alloys at all y and T_s values. This is consistent with the results reported in Ref. 12 showing that the concentration of substitutional C decreases with increasing dpa >0.14. Figure 6 shows that y_{sub} is negligible, irrespective of T_s for layers with total C concentrations $y \lesssim 0.010$ and grown with dpa=0.24. The concentration of substitutionally incorporated C only becomes significant in samples with dpa=0.24 when $y > 0.010$.

C. Layer strain

In this section we present the results of $Ge_{1-y}C_y$ strain measurements as a function of film growth parameters and show that they provide qualitative insight into C lattice site distributions. A quantitative analysis is carried out in Sec. V.

Figure 7 is a plot of the out-of-plane $Ge_{1-y}C_y$ lattice parameter $a_\perp$, obtained from HRRLMs, as a function of C concentration y for the four sets of growth conditions introduced in Fig. 6. The three dashed lines correspond to the lattice constants predicted by our density functional calculations assuming that C is incorporated solely in substitutional, Ge–C split interstitial, or nanocluster sites, respectively. The $Ge_{1-y}C_y$ layers grown at $T_s = 300\,°C$ with the low dpa value of 0.14 (closed squares) are all in a state of in-plane tension and the magnitude of the strain increases linearly with y. This observation is consistent with our Raman spectroscopy results (Fig. 6) showing an increase in the substitutional C concentration y_{sub} with increasing y. We note that all experimental data points are well above the calculated substitu-

Downloaded 28 Sep 2001 to 130.126.25.129. Redistribution subject to AIP license or copyright, see http://ojps.aip.org/japo/japcr.jsp

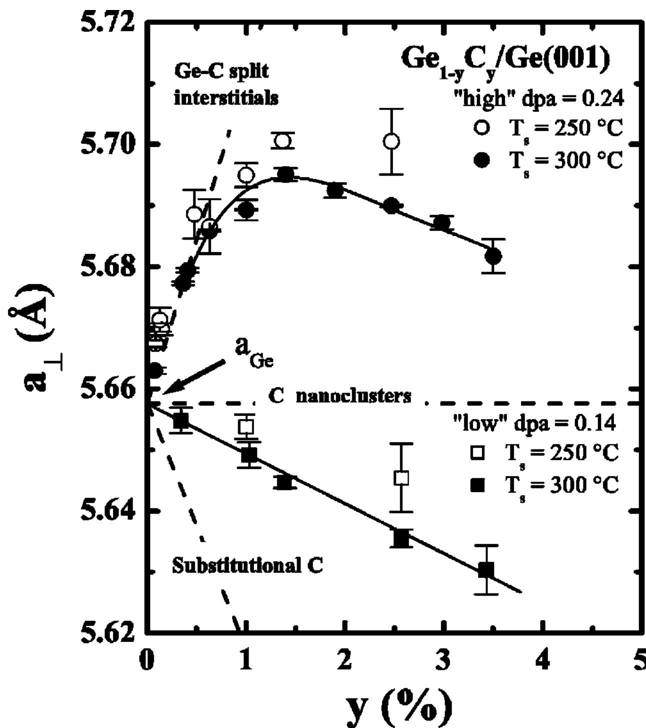

FIG. 7. Lattice parameter $a_\perp$ along the film growth direction vs the total C concentration y in $Ge_{1-y}C_y$/Ge(001) alloy layers. Open squares: dpa $=0.14$, $T_s=250\,°C$; closed squares: dpa=0.14; $T_s=300\,°C$; open circles: dpa=0.24, $T_s=250\,°C$; and closed circles: dpa=0.24, $T_s=300\,°C$. The dashed lines represent calculated $a_\perp(y)$ values for the three limiting cases in which all incorporated C atoms occupy either substitutional, Ge–C split interstitial, or nanocluster sites.

tional C line clearly indicating the additional presence of nonsubstitutional C atoms. More importantly, Fig. 7 shows that increasing the total C concentration in $Ge_{1-y}C_y$ alloys grown with low dpa values, irrespective of T_s, results in $a_\perp$ moving increasingly further above the substitutional C line.

For a given alloy concentration, the out-of-plane lattice constant $a_\perp$ moves even further above the substitutional C line for layers deposited at lower growth temperatures. However, Fig. 6 shows that y_{sub} increases with decreasing T_s. The increase in $a_\perp$ can therefore only be explained by a large increase in the fraction of C incorporated in split interstitials which induce compressive lattice strain and more than compensate the tensile strain associated with higher substitutional C incorporation at lower T_s.

HRRLM $a_\perp(y,T_s)$ results from $Ge_{1-y}C_y$ alloy layers grown at the high dpa are plotted in the upper part of Fig. 7. All high dpa films are in compression. Measured $a_\perp(y)$ values for alloys with C concentrations $y\leq 0.005$ at $T_s=300\,°C$ and $y\leq 0.007$ at $T_s=250\,°C$ are essentially equal to values calculated for samples in which all C atoms are incorporated as Ge–C split interstitials. This is strong evidence for complete C incorporation in split interstitial sites since C incorporation in any other site would lead to smaller $a_\perp$ values than we observe. At higher total C concentrations, the measured out-of-plane lattice parameters fall increasingly below the split interstitial line revealing the presence of C in sites with lower strain coefficients. For a given y, decreasing T_s from 300 to 250 °C with $y>0.007$ yields layers with higher compressive strain. Thus, as was the case for low dpa films, the Ge–C split interstitial concentration in $Ge_{1-y}C_y$ alloys decreases with increasing T_s.

V. DISCUSSION

$Ge_{1-y}C_y$ alloys grown from hyperthermal atom beams at temperatures of 250 and 350 °C, and containing C concentrations $y\leq 3.5$ at. %, are of excellent crystalline quality and fully coherent with their Ge(001) substrates as judged by HRRLM and XTEM. Moreover, XTEM investigations show that the layers contain no extended defects or C precipitates. Total C concentrations obtained from quantitative SIMS measurements agree well with values expected from growth rate calibrations and are constant as a function of depth in all layers, irrespective of T_s. Based on both our experimental results and *ab initio* density functional calculations, we have identified three types of C lattice configurations in our $Ge_{1-y}C_y$ films: substitutional C, Ge–C split interstitials, and C nanoclusters. The results in Fig. 7 clearly show that the layer strain, and thus the C lattice site distributions, strongly depend upon the total C concentration y, the growth temperature T_s, and the dpa.

We provide direct experimental evidence for C incorporation in substitutional and Ge–C split interstitial sites through Raman spectroscopy investigations and layer strain analyses, respectively. Ge–C split interstitials form due to substitutional C atoms trapping near-surface Ge self-interstitials Ge_I produced by the incident hyperthermal Ge atoms.[12] A similar reaction path was reported in electron-irradiated C-implanted Si where Si self-interstitials produced by the electron bombardment reacted with substitutional C atoms to produce Si–C split interstitials.[23] The Ge–C split interstitial configuration, with a formation energy per C atom 1.78 eV higher than that of substitutional C, becomes energetically favorable in the presence of Ge self-interstitials. We find that the Ge–C split interstitial formation energy associated with the reaction of substitutional C and Ge_I is -1.20 eV.

In the following, we combine our calculational and experimental results to determine quantitative C lattice site distributions in $Ge_{1-y}C_y$ layers. Using measured $Ge_{1-y}C_y$ lattice constants $a_\perp$ and substitutional C concentrations y_{sub} together with the calculated strain coefficients α, we employ Eqs. (2) and (3) to determine the C occupancy in substitutional, split interstitial, and nanocluster sites.

We first consider C lattice site distributions as a function of y and T_s for $Ge_{1-y}C_y$ films grown with low dpa. These layers contain significant substitutional C concentrations as determined by Raman spectroscopy. Figure 8(a) shows that the substitutional C fraction ξ_{sub} in layers grown at $T_s=300\,°C$ is 0.67 at low total concentrations, $y=0.003$, but decreases rapidly with increasing y. The C fraction ξ_{split} incorporated as Ge–C split interstitials in these layers [Fig. 8(b)] also decreases with y, ranging from 0.33 with $y=0.003$ to essentially zero with $y\geq 0.025$. In contrast, Fig. 8(c) shows that the fraction $\xi_{cluster}$ of C in nanoclusters increases rapidly with increasing total C concentration y from zero at low y values to 0.73 with $y=0.034$. That is, we ob-

Downloaded 28 Sep 2001 to 130.126.25.129. Redistribution subject to AIP license or copyright, see http://ojps.aip.org/japo/japcr.jsp

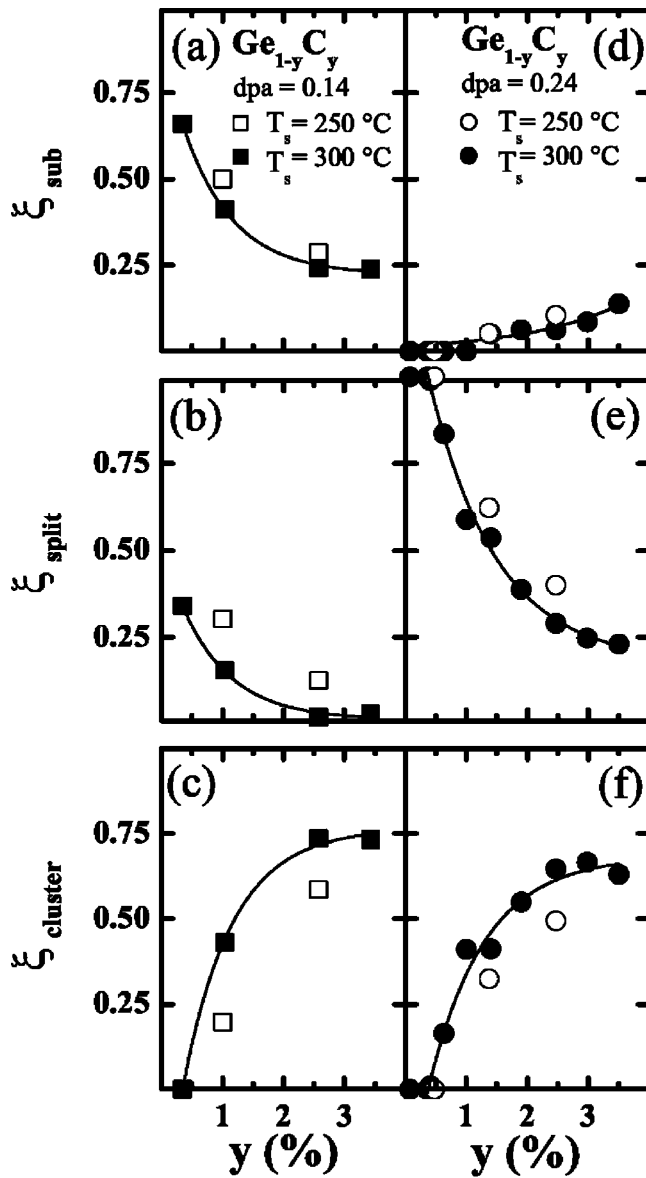

FIG. 8. The fractions of incorporated C in (a) substitutional sites ξ_{sub}, (b) split interstitial sites ξ_{split}, and (c) nanoclusters $\xi_{cluster}$ as a function of the total C concentration y in $Ge_{1-y}C_y(001)$ layers deposited using the low dpa value of 0.14 at $T_s = 250\,°C$ (open squares) and $T_s = 300\,°C$ (closed squares). (d)–(f) show corresponding data for $Ge_{1-y}C_y(001)$ layers grown with the high dpa of 0.24.

serve a decrease in the fraction of C incorporated in single-C configurations (substitutional C and Ge–C split interstitials) with increasing y due to increased incorporation in C nanoclusters. Both ξ_{sub} and ξ_{split} are slightly higher in layers grown at lower temperatures (Fig. 8, open symbols). Thus increasing y and/or T_s in layers grown with a low dpa favors the incorporation of C in nanoclusters.

These results are consistent with our density functional calculations showing that C nanoclusters are significantly more stable than either substitutional C or Ge–C split interstitials. In fact, based on formation energy considerations alone, all C atoms should reside in nanoclusters. The fact that C atoms do occupy single-C configurations whose fractional concentrations in $Ge_{1-y}C_y$ increase with decreases in y and T_s [Figs. 8(a) and 8(b)] suggests that C nanocluster formation is kinetically limited by the encounter probability of C atoms on the growth surface. Bulk diffusion of C in Ge is negligible at the temperatures used in these experiments.[24]

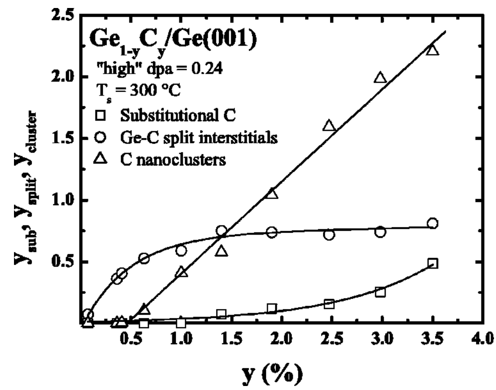

FIG. 9. C concentrations of incorporated C in substitutional sites y_{sub} (squares), split interstitial sites y_{split} (circles), and nanoclusters $y_{cluster}$ (triangles) as a function of the total C concentration y in $Ge_{1-y}C_y(001)$ layers deposited using the high dpa value of 0.24 at $T_s = 300\,°C$.

We now turn our attention to the high dpa samples [Figs. 8(d)–8(f)]. We find that just as in the case of the low dpa layers, the fraction of nanoclusters increases with increasing total C concentration and film growth temperature [Fig. 8(f)]. There are, however, significant differences in C lattice site distributions. $Ge_{1-y}C_y$ alloys grown with the high dpa exhibit much larger Ge–C split interstitial concentrations [Fig. 8(e)]. As discussed above, increasing the dpa leads to a higher concentration of Ge self-interstitials Ge_I in the near-surface region, and hence an enhanced concentration of Ge–C split interstitials due to trapping of Ge_I by substitutional C atoms. As a result, the substitutional C fraction ξ_{sub}, for a given $Ge_{1-y}C_y$ alloy concentration ($y \leq 0.035$), decreases [compare Figs. 8(d) and 8(a)] while the split interstitial fraction ξ_{split} increases [compare Figs. 8(e) and 8(b)] with increasing dpa.

At very low C concentrations, $y \lesssim 0.005$ in the high dpa samples, essentially all C is incorporated in Ge–C split interstitials. Even with increasing y up to $\simeq 0.010$, ξ_{sub} remains negligible. However, ξ_{split} decreases rapidly as C begins to incorporate in nanoclusters at $y > 0.005$. At still higher C concentrations, $y > 0.010$, ξ_{sub} begins to increase slowly, ξ_{split} continues to decrease rapidly, and $\xi_{cluster}$ increases rapidly. We note that even though the fraction ξ_{split} of C incorporated in split interstitials decreases, the concentration y_{split} increases with y until it reaches saturation at $y_{split} \simeq 0.007$ for $y > 0.010$. This is shown in Fig. 9, a plot of y_{sub}, y_{split}, and $y_{cluster}$ vs y for $Ge_{1-y}C_y$ alloys grown at $T_s = 300\,°C$ with the high dpa. The saturation in y_{split} suggests that even for $Ge_{1-y}C_y$ layers grown at high dpa, the near-surface Ge self-interstitial concentration is not large enough to convert all substitutional C atoms into Ge–C split interstitials. Thus ξ_{sub} increases continuously with increasing $y > 0.010$. Figure 9 also shows that the C concentration incorporated in nanoclusters increases with increasing y. Overall, the fraction of incorporated C residing in single-C configurations (the sum of ξ_{sub} and ξ_{split}) decreases with both increasing y and higher T_s in high dpa samples, just as for low dpa layers, consistent

Downloaded 28 Sep 2001 to 130.126.25.129. Redistribution subject to AIP license or copyright, see http://ojps.aip.org/japo/japcr.jsp

with our proposed mechanisms for the formation of C nanoclusters being kinetically limited by the C–C encounter probability at the growth surface during deposition.

VI. CONCLUSIONS

In summary, we have grown commensurate epitaxial $Ge_{1-y}C_y$ alloys on Ge(001) with C concentrations up to 3.5 at % at temperatures of 250 and 300 °C. The layers were deposited from hyperthermal beams in order to probe C incorporation pathways. HRRLM and XTEM analyses show that the layers contain no detectable extended defects or C precipitates. The combination of *ab initio* density functional calculations, SIMS, Raman spectroscopy, and HRRLM was used to quantitatively determine the concentrations of C incorporated in substitutional, split interstitial, and nanocluster sites as a function of film growth conditions: y, T_s, and dpa.

Based upon the overall set of calculations and experimental results we propose the following mechanisms, as a function of deposition conditions, for C incorporation in commensurate $Ge_{1-y}C_y$ alloys grown on Ge(001). At low total C concentrations and growth temperatures, all C atoms are incorporated in single-C configurations. In the absence of a significant Ge self-interstitial population (created in our case through growth from hyperthermal beams with controllable energy distributions), the incorporation of substitutional C is strongly favored due to its formation energy being 1.78 eV lower than that of Ge–C split interstitials. Thus, C is primarily incorporated in substitutional lattice sites in the low-dpa $Ge_{1-y}C_y$ samples grown at low T_s with small y values. Increasing the dpa through increases in the incident hyperthermal energy distribution yields a higher formation rate of Ge self-interstitials, thereby resulting in a corresponding increase in the Ge–C split interstitial concentration, through capture of Ge interstitials by substitutional C, and a decrease in the residual substitutional C concentration. Conversely, we do not expect significant split interstitial concentrations in $Ge_{1-y}C_y$ alloys from thermal beams (e.g., MBE), irrespective of the total C concentration or film growth temperature.

As the total C concentration y and film growth temperatures T_s increase, our layer strain analyses clearly indicate that C atoms incorporate in nanocluster sites. This is consistent with the results of our *ab initio* calculations showing that the nanocluster formation energies per C atom are lower than those of C in the single-carbon substitutional and Ge–C split interstitial configurations. Quantitative C lattice site distributions reveal that the fraction of C atoms incorporated in nanocluster sites increases rapidly with increasing total C concentration y and film growth temperature T_s. This shows that nanocluster formation is kinetically limited by the C–C adatom encounter probability which increases with both y and T_s.

ACKNOWLEDGMENTS

The authors gratefully acknowledge the financial support of the Materials Science Division of the Department of Energy under Contract No. DEFG02-96ER45439. They also appreciate the use of the facilities of the Center for Microanalysis of Materials, which is partially supported by the DOE, at the University of Illinois. J.D.-G. and P.D. were partially supported by the Natural Sciences and Engineering Research Council of Canada and the Fonds pour la Formation de chercheurs et à l'aide à la recherche (Québec, Canada).

[1] R. I. Scace and G. A. Slack, J. Chem. Phys. **30**, 1551 (1959).
[2] J. Tersoff, Phys. Rev. Lett. **74**, 5080 (1995).
[3] R. Duschl, O. G. Schmidt, W. Winter, K. Eberl, M. W. Dashiell, J. Kolodzey, N. Y. Jin-Phillipp, and F. Phillipp, Appl. Phys. Lett. **74**, 1150 (1999).
[4] M. W. Dashiell, J. Kolodzey, P. Boucaud, V. Yam, and J.-M. Lourtioz, J. Vac. Sci. Technol. B **18**, 1728 (2000).
[5] B.-K. Yang, M. Krishnamurthy, and W. H. Weber, J. Appl. Phys. **82**, 3287 (1997).
[6] W. H. Weber, B.-K. Yang, and M. Krishnamurthy, Appl. Phys. Lett. **73**, 626 (1998).
[7] L. Hoffman, J. C. Bach, B. B. Nielsen, P. Leary, R. Jones, and S. Öberg, Phys. Rev. B **55**, 11167 (1997).
[8] P. C. Kelires, Phys. Rev. B **60**, 10837 (1999).
[9] C. Guedj, J. Kolodzey, and A. Hairie, Phys. Rev. B **60**, 15150 (1999).
[10] J. Tersoff, Phys. Rev. Lett. **64**, 1757 (1990).
[11] D. Gall, J. D'Arcy-Gall, and J. E. Greene, Phys. Rev. B **62**, 7723 (2000).
[12] J. D'Arcy-Gall, D. Gall, P. Desjardins, I. Petrov, and J. E. Greene, Phys. Rev. B **62**, 11203 (2000).
[13] J. F. Ziegler, J. P. Biersack, and U. Littmark, *Stopping and Ranges of Ions in Solids* (Pergamon, New York, 1985).
[14] N.-E. Lee, M. Matsuoka, M. R. Sardela, Jr., F. Tian, and J. E. Greene, J. Appl. Phys. **80**, 812 (1996).
[15] G. A. Tomasch, Y.-W. Kim, L. C. Markert, N.-E. Lee, and J. E. Greene, Thin Solid Films **223**, 212 (1993).
[16] X.-J. Zhang, G. Xue, A. Agarwal, R. Tsu, M.-A. Hasan, J. E. Greene, and A. Rockett, J. Vac. Sci. Technol. A **11**, 2553 (1993).
[17] J. P. Noel, N. Hirashita, L. C. Markert, Y.-W. Kim, J. E. Greene, J. Knall, W.-X. Ni, M. A. Hasan, and J.-E. Sundgren, J. Appl. Phys. **65**, 1189 (1989).
[18] D. E. Aspnes and A. A. Studna, Phys. Rev. B **27**, 985 (1983).
[19] G. Kresse and J. Hafner, Phys. Rev. B **47**, 558 (1993); **49**, 14251 (1994); G. Kresse and J. Furthmüller, Comput. Mater. Sci. **6**, 15 (1996); Phys. Rev. B **54**, 11169 (1996).
[20] D. Vanderbilt, Phys. Rev. B **41**, 7892 (1990).
[21] J. P. Perdew and Y. Wang, Phys. Rev. B **45**, 13244 (1992).
[22] P. Brüesch, *Phonons: Theory and Experiments I* (Springer-Verlag, Berlin, 1982), p. 129.
[23] G. Davies and R. C. Newman, in *Handbook on Semiconductors*, edited by S. Mahajan (Elsevier, New York, 1994), Vol. 3, p. 1557.
[24] See annealing experiments in: J. D'Arcy-Gall, P. Desjardins, I. Petrov, J. E. Greene, J.-E. Paultre, R. A. Masut, S. C. Gujrathi, and S. Roorda, J. Appl. Phys. **88**, 96 (2000).

Downloaded 28 Sep 2001 to 130.126.25.129. Redistribution subject to AIP license or copyright, see http://ojps.aip.org/japo/japcr.jsp